

Minkowski functionals and the nonlinear perturbation theory in the large-scale structure: Second-order effects

Takahiko Matsubara^{1,2,*}, Chiaki Hikage^{3,†} and Satoshi Kuriki^{4,5,‡}

¹*Institute of Particle and Nuclear Studies, High Energy Accelerator Research Organization (KEK), Oho 1-1, Tsukuba 305-0801, Japan*

²*The Graduate University for Advanced Studies (SOKENDAI), Tsukuba, Ibaraki 305-0801, Japan*

³*Kavli Institute for the Physics and Mathematics of the Universe (Kavli IPMU, WPI), University of Tokyo, 5-1-5 Kashiwanoha, Kashiwa, Chiba 277-8583, Japan*

⁴*Institute of Statistical Mathematics, Research Organization of Information and Systems, 10-3 Midoricho, Tachikawa, Tokyo 190-8562, Japan*

⁵*The Graduate University for Advanced Studies (SOKENDAI), Tachikawa, Tokyo 190-8562, Japan*



(Received 2 December 2020; accepted 11 January 2022; published 24 January 2022)

The second-order formula of Minkowski functionals in weakly non-Gaussian fields is compared with the numerical N -body simulations. Recently, the weakly non-Gaussian formula of Minkowski functionals is extended to include the second-order effects of non-Gaussianity in general dimensions. We apply this formula to the three-dimensional density field in the large-scale structure of the Universe. The parameters of the second-order formula include several kinds of skewness and kurtosis parameters. We apply tree level of nonlinear perturbation theory to estimate these parameters, including novel calculations of quartic cumulants. First we compare the theoretical values with those of numerical simulations on the basis of parameter values, and next we test the performance of the analytic formula combined with the perturbation theory. The second-order formula outperforms the first-order formula in general. The performance of the perturbation theory depends on the smoothing radius applied in defining the Minkowski functionals. The quantitative comparisons are presented in detail.

DOI: [10.1103/PhysRevD.105.023527](https://doi.org/10.1103/PhysRevD.105.023527)

I. INTRODUCTION

The large-scale structure of the Universe has rich information for cosmology. The structure originates from the initial density fluctuations, which are believed to be generated by the cosmic inflation in the very early universe [1–4]. While many scenarios to achieve the inflation are proposed so far [5], we still do not know the true mechanism to generate the initial density field. The large-scale structure of the Universe also contains information about the evolution of the Universe. Such cosmological information is contained in the statistical properties of the large-scale structure, and therefore it is of great importance to statistically characterize the observed structures.

The power spectrum (and its Fourier counterpart, correlation function) is one of the most popular statistics to characterize the large-scale structure [6]. The statistical properties of a random Gaussian field are completely characterized once the power spectrum is specified. The large-scale structure is nearly Gaussian on sufficiently large scales, or at sufficiently early time, since the initial

conditions of the density fluctuations are nearly Gaussian as indicated by the cosmic microwave background radiation [7]. However, gravitational evolutions destroy the Gaussianity of the distribution, and non-Gaussianity comes in on small scales in late time.

How to effectively characterize the non-Gaussian fields is a nontrivial problem in cosmology. This problem attracts a lot of attention because the power spectrum or correlation function cannot capture the information about the non-Gaussianity. One of the straightforward ways to characterize the non-Gaussianity is to consider higher-order generalizations of the power spectrum and correlation function, i.e., polyspectra and N -point correlation functions. Nevertheless, these higher-order correlations are difficult to accurately measure, because these are functions of scales with many arguments [6]. There are many alternative methods to characterize the non-Gaussianity in general.

Among others, the set of Minkowski functionals [8,9] is one of the popular methods to investigate the non-Gaussianity in cosmology [10,11]. Applications of the Minkowski functionals to the large-scale structure of the Universe are also quite popular [12–22]). The Minkowski functionals are calculated for the excursion set of the random fields, such as isodensity surfaces of the large-scale structure. The isodensity surfaces are defined by

*tmats@post.kek.jp

†chiaki.hikage@ipmu.jp

‡kuriki@ism.ac.jp

specifying the density threshold, and the Minkowski functionals are considered as functions of the threshold for a given density field.

One of the striking properties of the Minkowski functionals is the fact that the functional forms of the Minkowski functionals as functions of the threshold have universal forms for Gaussian random fields: according to Tomita's formula [23], the Minkowski functionals of random Gaussian fields are represented by specific functions which are common to all random Gaussian fields. Only the amplitudes of the functions are affected by the power spectrum of the distributions. Thus, any deviation from the Gaussian predictions of the Minkowski functionals as functions of the threshold indicates non-Gaussianity of the distribution.

Interpreting the deviations from the Gaussian predictions of the Minkowski functionals is theoretically important to understand the nature of non-Gaussianity. The theoretical models for the generation mechanisms of initial density fluctuations usually predict the higher-order polyspectra such as the bispectrum, trispectrum, and so forth. The relation between the non-Gaussian Minkowski functionals and higher-order polyspectra are analytically derived with an expansion scheme when the non-Gaussianity is weak [24,25]. The first-order corrections of the non-Gaussianity in the Minkowski functionals are solely determined by integrals of the bispectrum, which are called skewness parameters. Until recently, the analytic formula of the first-order corrections to the Minkowski functionals are derived in three or less dimensions. The second-order corrections depend both on bispectrum and trispectrum. The analytic formula with second-order corrections in two dimensions is derived [26]. Formal expression of Euler characteristic, or genus statistics, which is one of the Minkowski functionals, in two and three dimensions in terms of the Gram-Charlier expansion to all orders are known [27,28]. Most recently, an analytic formula for non-Gaussian corrections up to the second order are derived in general dimensions [29,30]. The second-order terms involve integrals of trispectrum, which are called kurtosis parameters. Concrete relations of the second-order corrections to the bispectrum and trispectrum are derived in the last literature.

In this paper, we address how the second-order formula works in the analysis of the large-scale structure in three dimensions. For this purpose, we employ both the nonlinear perturbation theory and N -body simulations of gravitational evolution in the expanding Universe. Nonlinear perturbation theory is expected to be valid in the weakly nonlinear regime on large scales, while the N -body simulations can probe the fully nonlinear regime at the expense of computational cost. The comparison between the perturbation theory and numerical simulations gives a useful insight into the applicability of the analytic formula to realistic applications in cosmology.

This paper is organized as follows. In Sec. II, the second-order formula of Minkowski functionals are summarized, and many parameters in the formula are defined. In Sec. III, methods to evaluate skewness and kurtosis parameters by the nonlinear perturbation theory of gravitational evolution are developed. In Sec. IV, the analytic formula with the perturbation theory and the results of N -body simulations are compared in detail. Conclusions are given in Sec. V.

II. ANALYTIC FORMULA OF MINKOWSKI FUNCTIONALS WITH SECOND-ORDER NON-GAUSSIANITY

In this section, we summarize the second-order formula of Minkowski functionals with weak non-Gaussianity derived in the previous papers [29,30].

First we review mathematical definitions of Minkowski functionals in three-dimensional density fields $\rho(\mathbf{x})$ below [11]. We denote the density contrast by $\delta(\mathbf{x}) = \rho(\mathbf{x})/\bar{\rho} - 1$ where $\bar{\rho} = \langle \rho(\mathbf{x}) \rangle$ is the mean density. In cosmological applications, the Minkowski functionals are defined in smoothed density fields,

$$\delta_s(\mathbf{x}) = \int d^3x' W_R(|\mathbf{x} - \mathbf{x}'|) \delta(\mathbf{x}'), \quad (1)$$

where $W_R(x)$ is a smoothing kernel with smoothing radius R . It is a common practice to apply a Gaussian kernel,

$$W_R(x) = \frac{e^{-x^2/(2R^2)}}{(2\pi)^{3/2} R^3}, \quad (2)$$

to obtain the smoothed density field. We also assume this kernel function throughout this paper.

The Minkowski functionals are defined by specifying the isodensity contours with $\delta_s = \nu\sigma_0$, where ν is the threshold and

$$\sigma_0 = \langle \delta_s^2 \rangle^{1/2} \quad (3)$$

is the root-mean-square of the density fluctuations. There are four Minkowski functionals in three-dimensional space. We denote the Minkowski functionals per unit volume by $V_k(\nu)$ ($k = 0, 1, 2, 3$) as functions of the threshold ν which specifies the isodensity surfaces as defined below.

The Minkowski functional of $k = 0$ corresponds to the volume fraction of the excursion set,

$$V_0(\nu) = \frac{1}{V} \int_{F_\nu} d^3x, \quad (4)$$

where V is the total volume of the sample, and F_ν is a set of all positions which satisfies $\delta_s \geq \nu\sigma_0$. The other Minkowski functionals correspond to surface integrals of the isodensity surface ∂F_ν , which is the boundary of the excursion set,

$$V_k(\nu) = \frac{1}{V} \int_{\partial F_\nu} d^2x v_k(\nu, \mathbf{x}), \quad (5)$$

where $v_k(\nu, \mathbf{x})$ is the local Minkowski functionals defined by

$$v_1(\nu, \mathbf{x}) = \frac{1}{6}, \quad (6)$$

$$v_2(\nu, \mathbf{x}) = \frac{1}{6\pi} \left(\frac{1}{R_1} + \frac{1}{R_2} \right), \quad (7)$$

$$v_3(\nu, \mathbf{x}) = \frac{1}{4\pi} \frac{1}{R_1 R_2}, \quad (8)$$

and R_1, R_2 are the radii of curvature of the isodensity surface orientated toward lower density regions.

The Minkowski functionals have geometrical interpretations: the first Minkowski functional V_0 corresponds to the volume of the excursion set F_ν as described above. Minkowski functionals V_k with $k = 1, 2$ correspond to the area ($k = 1$) and the total mean curvature ($k = 2$) of the isodensity surface ∂F_ν , and V_3 corresponds the Euler characteristic which is a purely topological quantity.

Analytic formula of the Minkowski functionals up to second order in weakly non-Gaussian field in general dimensions d is derived in Refs. [29,30]. In the case of three dimensions, $d = 3$, the derived formula reduces to

$$\begin{aligned} V_k(\nu) = & \frac{1}{(2\pi)^{(k+1)/2}} \frac{\omega_3}{\omega_{3-k}\omega_k} \left(\frac{\sigma_1}{\sqrt{3}\sigma_0} \right)^k e^{-\nu^2/2} \left[\left[H_{k-1}(\nu) + \left[\frac{1}{6} S^{(0)} H_{k+2}(\nu) + \frac{k}{3} S^{(1)} H_k(\nu) + \frac{k(k-1)}{6} S^{(2)} H_{k-2}(\nu) \right] \sigma_0 \right. \right. \\ & + \left\{ \frac{1}{72} (S^{(0)})^2 H_{k+5}(\nu) + \left(\frac{1}{24} K^{(0)} + \frac{k}{18} S^{(0)} S^{(1)} \right) H_{k+3}(\nu) + k \left[\frac{1}{8} K^{(1)} + \frac{k-1}{36} S^{(0)} S^{(2)} + \frac{k-2}{18} (S^{(1)})^2 \right] H_{k+1}(\nu) \right. \\ & + k \left[\frac{k-2}{16} K_1^{(2)} + \frac{k}{16} K_2^{(2)} + \frac{(k-1)(k-4)}{18} S^{(1)} S^{(2)} \right] H_{k-1}(\nu) \\ & \left. \left. + k(k-1)(k-2) \left[\frac{1}{24} K^{(3)} + \frac{k-7}{72} (S^{(2)})^2 \right] H_{k-3}(\nu) \right\} \sigma_0^2 + \mathcal{O}(\sigma_0^3) \right], \quad (9) \end{aligned}$$

where $H_n(\nu) = e^{\nu^2/2} (-d/d\nu)^n e^{-\nu^2/2}$ are the probabilists' Hermite polynomials, and various parameters are given below in order. First, the factor

$$\omega_k \equiv \frac{\pi^{k/2}}{\Gamma(k/2 + 1)} \quad (10)$$

is the volume of the unit ball in k dimensions. Second,

$$\sigma_1 \equiv \langle \nabla \delta_s \cdot \nabla \delta_s \rangle^{1/2} \quad (11)$$

is a spectral moment. Third, $S^{(a)}$ are skewness parameters defined by

$$\begin{aligned} S^{(0)} &= \frac{\langle \delta_s^3 \rangle_c}{\sigma_0^4}, & S^{(1)} &= \frac{3}{2} \cdot \frac{\langle \delta_s |\nabla \delta_s|^2 \rangle_c}{\sigma_0^2 \sigma_1^2}, \\ S^{(2)} &= -\frac{9}{4} \cdot \frac{\langle |\nabla \delta_s|^2 \Delta \delta_s \rangle_c}{\sigma_1^4}, \end{aligned} \quad (12)$$

where $\langle \dots \rangle_c$ denotes the cumulants. However, all the third-order cumulants in the above equations can be replaced by simple means, because $\langle \delta_s \rangle = \langle \nabla \delta_s \rangle = 0$. Fourth, $K^{(a)}$ are kurtosis parameters defined by

$$K^{(0)} = \frac{\langle \delta_s^4 \rangle_c}{\sigma_0^6}, \quad K^{(1)} = 2 \cdot \frac{\langle \delta_s^2 |\nabla \delta_s|^2 \rangle_c}{\sigma_0^4 \sigma_1^2}, \quad (13)$$

$$K_1^{(2)} = -\frac{3}{5} \cdot \frac{5 \langle \delta_s |\nabla \delta_s|^2 \Delta \delta_s \rangle_c + \langle |\nabla \delta_s|^4 \rangle_c}{\sigma_0^2 \sigma_1^4}, \quad (14)$$

$$K_2^{(2)} = -\frac{3}{5} \cdot \frac{5 \langle \delta_s |\nabla \delta_s|^2 \Delta \delta_s \rangle_c + 3 \langle |\nabla \delta_s|^4 \rangle_c}{\sigma_0^2 \sigma_1^4}, \quad (15)$$

$$K^{(3)} = 9 \cdot \frac{\langle |\nabla \delta_s|^2 (\Delta \delta_s)^2 \rangle_c - \langle |\nabla \delta_s|^2 \delta_{s,ij} \delta_{s,ij} \rangle_c}{\sigma_1^6}, \quad (16)$$

where $\delta_{s,ij} \equiv \partial^2 \delta_s / \partial x_i \partial x_j$. The fourth-order cumulants are related to the mean values by

$$\langle \delta_s^4 \rangle_c = \langle \delta_s^4 \rangle - 3\sigma_0^4, \quad (17)$$

$$\langle \delta_s^2 |\nabla \delta_s|^2 \rangle_c = \langle \delta_s^2 |\nabla \delta_s|^2 \rangle - \sigma_0^2 \sigma_1^2, \quad (18)$$

$$\langle \delta_s |\nabla \delta_s|^2 \Delta \delta_s \rangle_c = \langle \delta_s |\nabla \delta_s|^2 \Delta \delta_s \rangle + \sigma_1^4, \quad (19)$$

$$\langle |\nabla \delta_s|^4 \rangle_c = \langle |\nabla \delta_s|^4 \rangle - \frac{5}{3} \sigma_1^4, \quad (20)$$

$$\langle |\nabla \delta_s|^2 (\Delta \delta_s)^2 \rangle_c = \langle |\nabla \delta_s|^2 (\Delta \delta_s)^2 \rangle - \sigma_1^2 \sigma_2^2, \quad (21)$$

$$\langle |\nabla \delta_s|^2 \delta_{s,ij} \delta_{s,ij} \rangle_c = \langle |\nabla \delta_s|^2 \delta_{s,ij} \delta_{s,ij} \rangle - \sigma_1^2 \sigma_2^2, \quad (22)$$

where

$$\sigma_2 \equiv \langle (\Delta\delta_s)^2 \rangle^{1/2} \quad (23)$$

is another spectral moment. The formula of Eq. (9) is a generalization of the analytic formula previously derived in restricted cases [23–26].

Various parameters in the formula of Eq. (9) are related to the power spectrum $P(k)$, bispectrum $B(\mathbf{k}_1, \mathbf{k}_2, \mathbf{k}_3)$, and trispectrum $T(\mathbf{k}_1, \mathbf{k}_2, \mathbf{k}_3, \mathbf{k}_4)$ of the (unsmoothed) density contrast δ , which are defined by

$$\langle \tilde{\delta}(\mathbf{k}) \tilde{\delta}(\mathbf{k}') \rangle_c = (2\pi)^3 \delta^3(\mathbf{k} + \mathbf{k}') P(k), \quad (24)$$

$$\langle \tilde{\delta}(\mathbf{k}_1) \tilde{\delta}(\mathbf{k}_2) \tilde{\delta}(\mathbf{k}_3) \rangle_c = (2\pi)^3 \delta^3(\mathbf{k}_1 + \mathbf{k}_2 + \mathbf{k}_3) B(\mathbf{k}_1, \mathbf{k}_2, \mathbf{k}_3), \quad (25)$$

$$\begin{aligned} \langle \tilde{\delta}(\mathbf{k}_1) \tilde{\delta}(\mathbf{k}_2) \tilde{\delta}(\mathbf{k}_3) \tilde{\delta}(\mathbf{k}_4) \rangle_c \\ = (2\pi)^3 \delta^3(\mathbf{k}_1 + \mathbf{k}_2 + \mathbf{k}_3 + \mathbf{k}_4) T(\mathbf{k}_1, \mathbf{k}_2, \mathbf{k}_3, \mathbf{k}_4), \end{aligned} \quad (26)$$

where

$$\tilde{\delta}(\mathbf{k}) = \int d^3x e^{-i\mathbf{k}\cdot\mathbf{x}} \delta(\mathbf{x}) \quad (27)$$

is the Fourier transform of the density contrast. The Fourier transform of the smoothed density contrast δ_s is given by $\tilde{\delta}_s(\mathbf{k}) = \tilde{\delta}(\mathbf{k}) W(kR)$, where

$$W(kR) = \int d^3x e^{-i\mathbf{k}\cdot\mathbf{x}} W_R(x) \quad (28)$$

is a (three-dimensional) Fourier transform of the smoothing kernel. In the case of Gaussian smoothing, Eq. (2), we have

$$W(kR) = e^{-k^2 R^2/2}. \quad (29)$$

The smoothed density contrast is therefore given by

$$\delta_s(\mathbf{x}) = \int \frac{d^3k}{(2\pi)^3} e^{i\mathbf{k}\cdot\mathbf{x}} \tilde{\delta}(\mathbf{k}) W(kR). \quad (30)$$

Substituting Eq. (30) into Eqs. (3), (11)–(16), (23), the spectral representations of the parameters are given by

$$\sigma_j^2 = \int \frac{d^3k}{(2\pi)^3} k^{2j} P(k) W^2(kR), \quad (31)$$

$$\begin{aligned} S^{(a)} &= \frac{1}{\sigma_0^{4-2a} \sigma_1^{2a}} \int \frac{d^3k_1}{(2\pi)^3} \frac{d^3k_2}{(2\pi)^3} \frac{d^3k_3}{(2\pi)^3} \\ &\times (2\pi)^3 \delta^3(\mathbf{k}_1 + \mathbf{k}_2 + \mathbf{k}_3) s^{(a)}(\mathbf{k}_1, \mathbf{k}_2, \mathbf{k}_3) \\ &\times B(\mathbf{k}_1, \mathbf{k}_2, \mathbf{k}_3) W(k_1 R) W(k_2 R) W(k_3 R), \end{aligned} \quad (32)$$

$$\begin{aligned} K^{(a)} &= \frac{1}{\sigma_0^{6-2a} \sigma_1^{2a}} \int \frac{d^3k_1}{(2\pi)^3} \frac{d^3k_2}{(2\pi)^3} \frac{d^3k_3}{(2\pi)^3} \frac{d^3k_4}{(2\pi)^3} \\ &\times (2\pi)^3 \delta^3(\mathbf{k}_1 + \mathbf{k}_2 + \mathbf{k}_3 + \mathbf{k}_4) \kappa^{(a)}(\mathbf{k}_1, \mathbf{k}_2, \mathbf{k}_3, \mathbf{k}_4) \\ &\times T(\mathbf{k}_1, \mathbf{k}_2, \mathbf{k}_3, \mathbf{k}_4) W(k_1 R) W(k_2 R) W(k_3 R) W(k_4 R), \end{aligned} \quad (33)$$

where

$$\begin{aligned} s^{(0)} &= 1, & s^{(1)} &= -\frac{3}{2} \mathbf{k}_1 \cdot \mathbf{k}_2, & s^{(2)} &= -\frac{9}{4} (\mathbf{k}_1 \cdot \mathbf{k}_2) k_3^2, \\ \kappa^{(0)} &= 1, & \kappa^{(1)} &= -2\mathbf{k}_1 \cdot \mathbf{k}_2, \\ \kappa_1^{(2)} &= -\frac{3}{5} (\mathbf{k}_1 \cdot \mathbf{k}_2) (5k_3^2 + \mathbf{k}_3 \cdot \mathbf{k}_4), \\ \kappa_2^{(2)} &= -\frac{3}{5} (\mathbf{k}_1 \cdot \mathbf{k}_2) (5k_3^2 + 3\mathbf{k}_3 \cdot \mathbf{k}_4), \\ \kappa^{(3)} &= -9(\mathbf{k}_1 \cdot \mathbf{k}_2) [k_3^2 k_4^2 - (\mathbf{k}_3 \cdot \mathbf{k}_4)^2]. \end{aligned} \quad (34)$$

Thus, all the necessary parameters in the formula of Eq. (9) are calculated once the power spectrum, bispectrum, and trispectrum of the density field are specified.

III. EVALUATING PARAMETERS BY THE NONLINEAR PERTURBATION THEORY

The cosmological perturbation theory of nonlinear density field [31] is one of the standard methods of evaluating the power spectrum and higher-order polyspectra in general. Therefore, it is natural to apply the perturbation theory to predict the parameters of the formula of non-Gaussian Minkowski functionals. In this section we derive the necessary equations to achieve the evaluations.

A. Spectra from the standard perturbation theory

In the standard perturbation theory, the nonlinear density contrast $\tilde{\delta}(\mathbf{k})$ in Fourier space is expanded by the linear density contrast $\delta_L(\mathbf{k})$ as

$$\begin{aligned} \tilde{\delta}(\mathbf{k}) &= \sum_{n=1}^{\infty} \frac{1}{n!} \int \frac{d^3k_1}{(2\pi)^3} \cdots \frac{d^3k_n}{(2\pi)^3} \delta_D^3(\mathbf{k}_1 + \cdots + \mathbf{k}_n - \mathbf{k}) \\ &\times F_n(\mathbf{k}_1, \dots, \mathbf{k}_n) \delta_L(\mathbf{k}_1) \cdots \delta_L(\mathbf{k}_n), \end{aligned} \quad (35)$$

and a similar expansion is applied to the velocity (divergence) field θ with kernel functions $G_n(\mathbf{k}_1, \dots, \mathbf{k}_n)$.¹ Using the recursion relations [31,32] of the kernels F_n and G_n , we have

¹Our conventions for the kernel functions F_n and G_n are different from most of the literature's in which a factor $1/n!$ in Eq. (35) is missing. One should replace $F_n, G_n \rightarrow n!F_n, n!G_n$ to reproduce the equations in the corresponding literature's. Our conventions designate most of the derived equations more concisely.

$$F_2(\mathbf{k}_1, \mathbf{k}_2) = \frac{10}{7} + \left(\frac{k_1}{k_2} + \frac{k_2}{k_1} \right) \frac{\mathbf{k}_1 \cdot \mathbf{k}_2}{k_1 k_2} + \frac{4}{7} \left(\frac{\mathbf{k}_1 \cdot \mathbf{k}_2}{k_1 k_2} \right)^2, \quad (36)$$

$$G_2(\mathbf{k}_1, \mathbf{k}_2) = \frac{6}{7} + \left(\frac{k_1}{k_2} + \frac{k_2}{k_1} \right) \frac{\mathbf{k}_1 \cdot \mathbf{k}_2}{k_1 k_2} + \frac{8}{7} \left(\frac{\mathbf{k}_1 \cdot \mathbf{k}_2}{k_1 k_2} \right)^2, \quad (37)$$

and

$$\begin{aligned} F_3(\mathbf{k}_1, \mathbf{k}_2, \mathbf{k}_3) &= \frac{7}{6} \alpha(\mathbf{k}_1, \mathbf{k}_2 + \mathbf{k}_3) F_2(\mathbf{k}_2, \mathbf{k}_3) \\ &+ \frac{1}{6} [7\alpha(\mathbf{k}_2 + \mathbf{k}_3, \mathbf{k}_1) \\ &+ 4\beta(\mathbf{k}_2 + \mathbf{k}_3, \mathbf{k}_1)] G_2(\mathbf{k}_2, \mathbf{k}_3), \end{aligned} \quad (38)$$

where

$$\alpha(\mathbf{k}_1, \mathbf{k}_2) \equiv 1 + \frac{\mathbf{k}_1 \cdot \mathbf{k}_2}{k_1^2}, \quad \beta(\mathbf{k}_1, \mathbf{k}_2) \equiv \frac{|\mathbf{k}_1 + \mathbf{k}_2|^2 (\mathbf{k}_1 \cdot \mathbf{k}_2)}{2k_1^2 k_2^2}. \quad (39)$$

Instead of the asymmetric kernel F_3 in the above equation, it is convenient to define the symmetrized kernel

$$F_3^{(s)}(\mathbf{k}_1, \mathbf{k}_2, \mathbf{k}_3) \equiv \frac{1}{3} F_3(\mathbf{k}_1, \mathbf{k}_2, \mathbf{k}_3) + \text{cyc}, \quad (40)$$

where “+cyc” denotes the cyclic permutations of the previous term with respect to the arguments $\mathbf{k}_1, \mathbf{k}_2, \mathbf{k}_3$.

In the lowest-order approximations (so-called “tree-level” approximations) of the perturbation theory, the power spectrum, bispectrum and trispectrum defined in Eqs. (24)–(26) are given by

$$P(k) = P_L(k), \quad (41)$$

$$B(\mathbf{k}_1, \mathbf{k}_2, \mathbf{k}_3) = F_2(\mathbf{k}_1, \mathbf{k}_2) P_L(k_1) P_L(k_2) + \text{cyc}, \quad (42)$$

$$\begin{aligned} T(\mathbf{k}_1, \mathbf{k}_2, \mathbf{k}_3, \mathbf{k}_4) &= F_2(\mathbf{k}_1, \mathbf{k}_2 + \mathbf{k}_3) F_2(\mathbf{k}_2, -\mathbf{k}_2 - \mathbf{k}_3) \\ &\times P_L(k_1) P_L(k_2) P_L(|\mathbf{k}_2 + \mathbf{k}_3|) + \text{sym}(11) \\ &+ F_3^{(s)}(\mathbf{k}_1, \mathbf{k}_2, \mathbf{k}_3) P_L(k_1) P_L(k_2) P_L(k_3) \\ &+ \text{sym}(3), \end{aligned} \quad (43)$$

where “+sym(n)” represents additional n terms to symmetrize the previous term with respect to the arguments $\mathbf{k}_1, \dots, \mathbf{k}_4$. Substituting Eqs. (41)–(43) and (34) into Eqs. (31)–(33), the parameters of the second-order formula (9) of Minkowski functionals are given in the tree-level perturbation theory of the gravitational evolution of density field. However, it is not straightforward to numerically evaluate the skewness and kurtosis parameters with the above equations as they involve higher-dimensional integrals. One can analytically reduce the dimensionality of

the integrals in order to practically evaluate them as we explain below.

B. Skewness and kurtosis parameters

The method to evaluate the skewness parameters $S^{(a)}$ with the Gaussian smoothing kernel in the perturbation theory are already known [24]. The simplest kurtosis $K^{(0)}$ with the Gaussian smoothing kernel are also already addressed [33]. We follow a similar, but somehow different approach to achieve the numerical evaluations of all the parameters. For that purpose, it turns out to be desirable to reexpress the integrals of skewness and kurtosis parameters, Eqs. (32) and (33). The functions $s^{(a)}$ and $\kappa^{(a)}$ can be replaced by the symmetrized ones,

$$\tilde{s}^{(a)}(\mathbf{k}_1, \mathbf{k}_2, \mathbf{k}_3) \equiv \frac{1}{3} s^{(a)}(\mathbf{k}_1, \mathbf{k}_2, \mathbf{k}_3) + \text{cyc}, \quad (44)$$

$$\tilde{\kappa}^{(a)}(\mathbf{k}_1, \mathbf{k}_2, \mathbf{k}_3, \mathbf{k}_4) \equiv \frac{1}{12} \kappa^{(a)}(\mathbf{k}_1, \mathbf{k}_2, \mathbf{k}_3, \mathbf{k}_4) + \text{sym}(11). \quad (45)$$

These functions are completely symmetric for any permutations of their arguments. When one replaces $s^{(a)} \rightarrow \tilde{s}^{(a)}$ and $\kappa^{(a)} \rightarrow \tilde{\kappa}^{(a)}$ in Eqs. (32) and (33), the bispectrum and trispectrum in the perturbation theory can be replaced by asymmetric functions,

$$\tilde{B}(\mathbf{k}_1, \mathbf{k}_2) \equiv 3F_2(\mathbf{k}_1, \mathbf{k}_2) P_L(k_1) P_L(k_2), \quad (46)$$

$$\begin{aligned} \tilde{T}(\mathbf{k}_1, \mathbf{k}_2, \mathbf{k}_3) &\equiv 12F_2(\mathbf{k}_1, \mathbf{k}_2 + \mathbf{k}_3) F_2(\mathbf{k}_2, -\mathbf{k}_2 - \mathbf{k}_3) \\ &\times P_L(k_1) P_L(k_2) P_L(|\mathbf{k}_2 + \mathbf{k}_3|) \\ &+ 4F_3(\mathbf{k}_1, \mathbf{k}_2, \mathbf{k}_3) P_L(k_1) P_L(k_2) P_L(k_3). \end{aligned} \quad (47)$$

Because of the delta functions in Eqs. (32) and (33), one can replace $\mathbf{k}_3 = -\mathbf{k}_1 - \mathbf{k}_2$ in Eq. (44) and $\mathbf{k}_4 = -\mathbf{k}_1 - \mathbf{k}_2 - \mathbf{k}_3$ in Eq. (45). We denote $\tilde{s}^{(a)}(\mathbf{k}_1, \mathbf{k}_2)$ and $\tilde{\kappa}^{(a)}(\mathbf{k}_1, \mathbf{k}_2, \mathbf{k}_3)$ after substituting these constraints. After all, Eqs. (32) and (33) are reexpressed as

$$\begin{aligned} S^{(a)} &= \frac{1}{\sigma_0^{4-2a} \sigma_1^{2a}} \int \frac{d^3 k_1}{(2\pi)^3} \frac{d^3 k_2}{(2\pi)^3} \tilde{s}^{(a)}(\mathbf{k}_1, \mathbf{k}_2) \\ &\times \tilde{B}(\mathbf{k}_1, \mathbf{k}_2) e^{-(k_1^2 + k_2^2 + \mathbf{k}_1 \cdot \mathbf{k}_2) R^2}, \end{aligned} \quad (48)$$

$$\begin{aligned} K^{(a)} &= \frac{1}{\sigma_0^{6-2a} \sigma_1^{2a}} \int \frac{d^3 k_1}{(2\pi)^3} \frac{d^3 k_2}{(2\pi)^3} \frac{d^3 k_3}{(2\pi)^3} \tilde{\kappa}^{(a)}(\mathbf{k}_1, \mathbf{k}_2, \mathbf{k}_3) \\ &\times \tilde{T}(\mathbf{k}_1, \mathbf{k}_2, \mathbf{k}_3) \\ &\times e^{-(k_1^2 + k_2^2 + k_3^2 + \mathbf{k}_1 \cdot \mathbf{k}_2 + \mathbf{k}_2 \cdot \mathbf{k}_3 + \mathbf{k}_3 \cdot \mathbf{k}_1) R^2}, \end{aligned} \quad (49)$$

where

$$\tilde{s}^{(0)} = 1, \quad (50)$$

$$\tilde{s}^{(1)} = \frac{1}{2}(k_1^2 + k_2^2 + \mathbf{k}_1 \cdot \mathbf{k}_2), \quad (51)$$

$$\tilde{s}^{(2)} = \frac{3}{2}[k_1^2 k_2^2 - (\mathbf{k}_1 \cdot \mathbf{k}_2)^2], \quad (52)$$

and

$$\tilde{\kappa}^{(0)} = 1, \quad (53)$$

$$\tilde{\kappa}^{(1)} = \frac{1}{3}(k_1^2 + k_2^2 + k_3^2 + \mathbf{k}_1 \cdot \mathbf{k}_2 + \mathbf{k}_2 \cdot \mathbf{k}_3 + \mathbf{k}_3 \cdot \mathbf{k}_1), \quad (54)$$

$$\begin{aligned} \tilde{\kappa}_1^{(2)} &= \frac{1}{10} \{5[k_1^2 k_2^2 - (\mathbf{k}_1 \cdot \mathbf{k}_2)^2] \\ &\quad - 6(\mathbf{k}_1 \cdot \mathbf{k}_3)(\mathbf{k}_2 \cdot \mathbf{k}_3) + 2(\mathbf{k}_1 \cdot \mathbf{k}_2)k_3^2\} + \text{cyc}, \end{aligned} \quad (55)$$

$$\begin{aligned} \tilde{\kappa}_2^{(2)} &= \frac{1}{10} \{5[k_1^2 k_2^2 - (\mathbf{k}_1 \cdot \mathbf{k}_2)^2] \\ &\quad + 2(\mathbf{k}_1 \cdot \mathbf{k}_3)(\mathbf{k}_2 \cdot \mathbf{k}_3) + 6(\mathbf{k}_1 \cdot \mathbf{k}_2)k_3^2\} + \text{cyc}, \end{aligned} \quad (56)$$

$$\begin{aligned} \tilde{\kappa}^{(3)} &= \frac{3}{2}[k_1^2 k_2^2 k_3^2 + 2(\mathbf{k}_1 \cdot \mathbf{k}_2)(\mathbf{k}_2 \cdot \mathbf{k}_3)(\mathbf{k}_3 \cdot \mathbf{k}_1) \\ &\quad - 3(\mathbf{k}_1 \cdot \mathbf{k}_2)^2 k_3^2] + \text{cyc}, \end{aligned} \quad (57)$$

and the Gaussian window function, Eq. (29), is explicitly used. In the lowest-order in the perturbation theory, the parameters σ_j of Eq. (31) are given by

$$\sigma_j^2 = \int_0^\infty \frac{k^2 dk}{2\pi^2} k^{2j} P_L(k) e^{-k^2 R^2}, \quad (58)$$

where the Gaussian window function is assumed.

Because the integrands of Eqs. (48) and (49) are rotationally invariant, one can reduce the dimensionality of the integrals by three dimensions. In order to reduce the dimensionality of integrals of Eq. (48) for the skewness parameters, one can choose the coordinates system,

$$\mathbf{k}_1 R = (p \sin \theta, 0, p \cos \theta), \quad \mathbf{k}_2 R = (0, 0, q), \quad (59)$$

and the volume element of the integral in Eq. (48) reduces to

$$\int \frac{d^3 k_1}{(2\pi)^3} \frac{d^3 k_2}{(2\pi)^3} \rightarrow \frac{1}{8\pi^4 R^6} \int_0^\infty p^2 dp \int_0^\infty q^2 dq \int_0^\pi \sin \theta d\theta. \quad (60)$$

We substitute Eqs. (46) and (50)–(52) into Eq. (48) in this coordinate system. The integral over the variable θ can analytically performed as

$$\int_0^\pi \sin \theta d\theta e^{x \cos \theta} \cos^n \theta = 2 \frac{d^n}{dx^n} \left(\frac{\sinh x}{x} \right). \quad (61)$$

As a result, we have expressions in a form,

$$\begin{aligned} S^{(a)} &= \frac{1}{8\pi^4 R^{2a+6} \sigma_0^{4-2a} \sigma_1^{2a}} \\ &\quad \times \int_0^\infty dp dq e^{-p^2 - q^2} \tilde{S}^{(a)}(p, q) P_L\left(\frac{p}{R}\right) P_L\left(\frac{q}{R}\right), \end{aligned} \quad (62)$$

where $\tilde{S}^{(a)}(p, q)$ are analytic functions which are explicitly given by

$$\tilde{S}^{(0)} = -6 \left(p^2 + q^2 + \frac{8}{7} \right) \cosh(pq) + 6 \left(2p^2 q^2 + p^2 + q^2 + \frac{8}{7} \right) \frac{\sinh(pq)}{pq}, \quad (63)$$

$$\tilde{S}^{(1)} = -3 \left[p^4 + q^4 + 4p^2 q^2 + \frac{22}{7}(p^2 + q^2) + \frac{24}{7} \right] \cosh(pq) + 3 \left[\left(3p^2 q^2 + \frac{22}{7} \right) (p^2 + q^2) + p^4 + q^4 + \frac{36}{7} p^2 q^2 + \frac{24}{7} \right] \frac{\sinh(pq)}{pq}, \quad (64)$$

$$\tilde{S}^{(2)} = 18 \left[2p^2 q^2 + 3(p^2 + q^2) + \frac{48}{7} \right] \cosh(pq) - 18 \left[(p^2 q^2 + 3)(p^2 + q^2) + \frac{30}{7} p^2 q^2 + \frac{48}{7} \right] \frac{\sinh(pq)}{pq}. \quad (65)$$

The two-dimensional integrations of Eq. (62) are numerically evaluated without any difficulty.

Similarly, the dimensionality of integrals of Eq. (49) for kurtosis parameters can be reduced due to the rotational invariance of integrands. It is convenient to change the integration variables [33],

$$\mathbf{p} = \mathbf{k}_1 R, \quad \mathbf{q} = \mathbf{k}_2 R, \quad \mathbf{r} = (\mathbf{k}_2 + \mathbf{k}_3) R, \quad (66)$$

or,

$$\mathbf{k}_1 = \frac{\mathbf{p}}{R}, \quad \mathbf{k}_2 = \frac{\mathbf{q}}{R}, \quad \mathbf{k}_3 = \frac{\mathbf{r} - \mathbf{q}}{R}. \quad (67)$$

One can choose coordinates system,

$$\mathbf{p} = (p \sin \theta \cos \phi, p \sin \theta \sin \phi, p \cos \theta), \quad (68)$$

$$\mathbf{q} = (q \sin \theta', 0, q \cos \theta'), \quad \mathbf{r} = (0, 0, r). \quad (69)$$

and the volume element of the integral in Eq. (49) reduces to

$$\begin{aligned} & \int \frac{d^3 k_1}{(2\pi)^3} \frac{d^3 k_2}{(2\pi)^3} \frac{d^3 k_3}{(2\pi)^3} \\ & \rightarrow \frac{1}{32\pi^6 R^9} \int_0^\infty p^2 dp \int_0^\infty q^2 dq \int_0^\infty r^2 dr \\ & \quad \times \int_0^\pi \sin \theta d\theta \int_0^\pi \sin \theta' d\theta' \int_0^{2\pi} \frac{d\phi}{2\pi}. \end{aligned} \quad (70)$$

The integral over the variable ϕ is straightforward, and the integral over θ can again analytically performed by applying Eq. (61). The integrals over θ' are only possible for the first term of Eq. (47), and are not possible for the second term. We use a new integration variable $\mu = \cos \theta'$ for the last integrals. As a result, we have expressions in a form,

$$\begin{aligned} K^{(a)} = & \frac{1}{32\pi^6 R^{2a+9} \sigma_0^{6-2a} \sigma_1^{2a}} \int_0^\infty dp dq dr e^{-p^2 - q^2 - r^2} \\ & \times \left[\tilde{K}^{(a)}(p, q, r) P_L\left(\frac{p}{R}\right) P_L\left(\frac{q}{R}\right) P_L\left(\frac{r}{R}\right) \right. \\ & + \int_{-1}^1 d\mu e^{qr\mu} \tilde{L}^{(a)}(p, q, r, \mu) P_L\left(\frac{p}{R}\right) P_L\left(\frac{q}{R}\right) \\ & \left. \times P_L\left(\frac{\sqrt{q^2 + r^2 - 2qr\mu}}{R}\right) \right], \end{aligned} \quad (71)$$

where $\tilde{K}^{(a)}$, $\tilde{L}^{(a)}$ are analytic functions. For example,

$$\begin{aligned} \tilde{K}^{(0)} = & \frac{48}{r^2} \left[\left(p^2 + r^2 + \frac{8}{7} \right) \cosh(pr) - \left(2p^2 r^2 + p^2 + r^2 + \frac{8}{7} \right) \frac{\sinh(pr)}{pr} \right] \\ & \times \left[\left(q^2 + r^2 + \frac{8}{7} \right) \cosh(qr) - \left(2q^2 r^2 + q^2 + r^2 + \frac{8}{7} \right) \frac{\sinh(qr)}{qr} \right], \end{aligned} \quad (72)$$

$$\begin{aligned} \tilde{L}^{(0)} = & \frac{4qr^2}{21(q^2 + r^2 - 2qr\mu)} \left\{ [(8 + 9p^2 - 19r^2)q - 7(8 + 9p^2 + 9r^2)r\mu + 2(24 + 27p^2 + 41r^2)q\mu^2] \cosh(pr) \right. \\ & - [(8 + 9p^2 - 19r^2 - 10p^2 r^2)q - 7(8 + 9p^2 + 9r^2 + 18p^2 r^2)r\mu \\ & \left. + 2(24 + 27p^2 + 41r^2 + 68p^2 r^2)q\mu^2] \frac{\sinh(pr)}{pr} \right\}. \end{aligned} \quad (73)$$

Other functions $\tilde{K}^{(1)}$, $\tilde{K}_1^{(2)}$, $\tilde{K}_2^{(2)}$, $\tilde{K}^{(3)}$ are similarly given, although explicit expressions of these functions are too tedious to reproduce here. It is straightforward to derive the expressions by using the *Mathematica* package. With these analytic results, we numerically evaluate the three- and four-dimensional integrations of Eq. (71).

IV. COMPARISONS WITH NUMERICAL SIMULATIONS

To see how the non-Gaussian formula of Minkowski functionals works in the three-dimensional large-scale structure, we now compare the analytic predictions and the results of cosmological N -body simulations. For that purpose, we calculate the Minkowski functionals from 300 realizations of the N -body simulations from the Quijote suite [34]. Each realization contains $N = 512^3$ particles in a box size of $V = 1 h^{-3} \text{Gpc}^3$. The cosmological parameters of the simulations are given by $\Omega_m = 0.3175$, $\Omega_b = 0.049$, $h = 0.6711$, $n_s = 0.9624$, $\sigma_8 = 0.834$, and a flat Λ CDM model is assumed. In calculating the Minkowski

functionals, the density field in the simulation box is smoothed by a Gaussian filter of the radius $R = 10, 20, 30, 40 h^{-1} \text{Mpc}$. The Minkowski functionals are numerically evaluated based on Crofton's formula from integral geometry [35,36] where each Minkowski functional can be computed by counting the numbers of vertices, edges, faces, and cubes of the excursion set over a threshold ν [11].

With the same set of cosmological parameters, theoretical predictions of the weakly non-Gaussian formula of Minkowski functionals with the nonlinear perturbation theory are calculated according to the method described in the previous section. The linear power spectrum $P_L(k)$ is evaluated by the CLASS code [37,38]. Once the linear power spectrum is given, all the parameters in the formula of Eq. (9) for the Minkowski functionals are calculated by numerical integrations of Eqs. (58), (62), (71).

In Table I, the parameters of the weakly non-Gaussian formula of Minkowski functionals are given. The upper figures of each entry represent the predictions of the

TABLE I. The values of parameters for the weakly non-Gaussian formula of Minkowski functionals in the large-scale structure. Four cases of the smoothing radius R are presented. The values calculated from the lowest-order perturbation theory (upper figures) and directly from the numerical simulations with 1σ errors (lower figures) are listed.

R [h^{-1} Mpc]	10	20	30	40
σ_0	0.385 0.3804 ± 0.0001	0.193 0.1899 ± 0.0001	0.121 0.1194 ± 0.0001	0.0845 0.08374 ± 0.0001
σ_1	0.0367 0.03652 ± 0.00001	0.0101 0.009918 ± 0.000004	0.00441 0.004352 ± 0.000003	0.00240 0.002371 ± 0.000002
$S^{(0)}$	3.56 3.762 ± 0.004	3.40 3.46 ± 0.01	3.33 3.36 ± 0.02	3.28 3.28 ± 0.05
$S^{(1)}$	3.63 3.932 ± 0.003	3.45 3.531 ± 0.006	3.36 3.41 ± 0.01	3.31 3.34 ± 0.03
$S^{(2)}$	3.66 4.499 ± 0.004	3.68 3.887 ± 0.006	3.71 3.81 ± 0.01	3.72 3.78 ± 0.03
$K^{(0)}$	23.2 26.66 ± 0.09	20.9 21.6 ± 0.2	19.9 20.2 ± 0.5	19.2 19 ± 1
$K^{(1)}$	23.8 28.77 ± 0.09	21.3 22.2 ± 0.1	20.2 20.6 ± 0.3	19.5 19.8 ± 0.8
$K_1^{(2)}$	30.6 41.7 ± 0.1	28.3 30.4 ± 0.2	27.2 28.1 ± 0.4	26.7 27.5 ± 0.8
$K_2^{(2)}$	18.8 26.7 ± 0.1	17.7 19.2 ± 0.1	17.3 18.0 ± 0.2	17.0 17.8 ± 0.6
$K^{(3)}$	25.1 45.5 ± 0.2	25.6 29.6 ± 0.2	26.1 27.6 ± 0.4	26.4 27 ± 1

lowest-order perturbation theory. The lower figures of each entry are the values calculated directly from the simulation data with Eqs. (3), (11)–(23). In Figs. 1, 2 and 3, the values of various parameters calculated from the perturbation theory and simulation data are compared. The spectral parameters σ_j in the simulations are well reproduced by the tree-level perturbation theory within a few percent on every scale. The skewness and kurtosis parameters in the simulations are quantitatively reproduced by the tree-level perturbation theory on sufficiently large scales within 5%

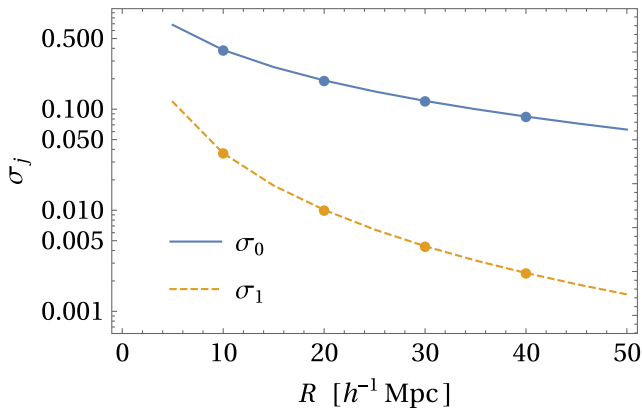


FIG. 1. The values of σ_0 and σ_1 calculated from the perturbation theory (solid and dashed lines, respectively) and simulation data (points with error bars), as functions of smoothing radius R .

for $R \gtrsim 30 h^{-1}$ Mpc, while the accuracy of the perturbation theory decreases to 10% for $R \sim 20 h^{-1}$ Mpc and much worse for $R \sim 10 h^{-1}$ Mpc.

Finally, the Minkowski functionals calculated from the numerical simulations are compared with analytic predictions in Figs. 4–7. Each figure corresponds to different smoothing radius. The symbols represent the measured values and errors estimated from the 300 realizations of simulations. The leftmost columns show the shape of the

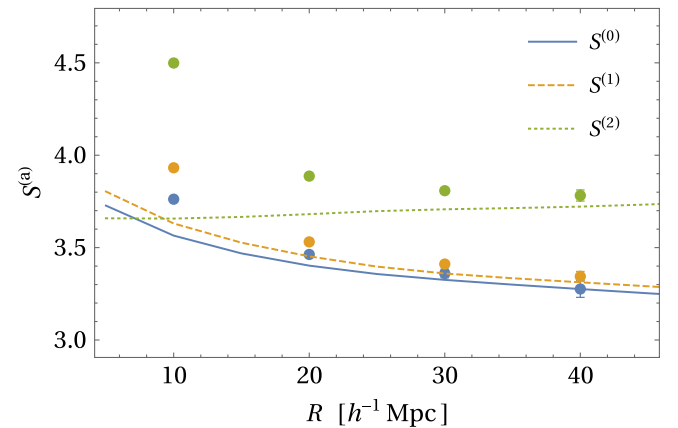


FIG. 2. The values of skewness parameters $S^{(0)}$, $S^{(1)}$, $S^{(2)}$ calculated from the perturbation theory (solid, dashed and dotted lines, respectively) and simulation data (points with error bars), as functions of smoothing radius R .

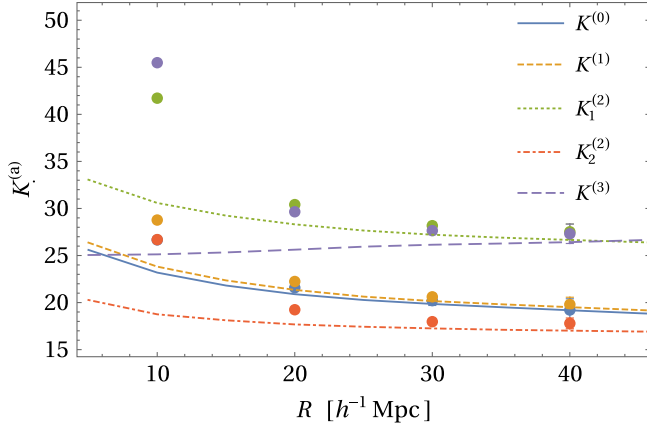


FIG. 3. The values of kurtosis parameters $K^{(0)}$, $K^{(1)}$, $K_1^{(2)}$, $K_2^{(2)}$, $K^{(3)}$ calculated from the perturbation theory (solid, dashed, dotted, dash-dotted and long-dashed lines, respectively) and simulation data (points with error bars), as functions of smoothing radius R .

Minkowski functionals. The second and third columns show the differences from the Gaussian predictions, i.e., they depict the non-Gaussian effects. The numerical results (symbols) in these two columns are the same. The Gaussian predictions are subtracted from the full Minkowski functionals. Only the theoretical predictions (solid and dashed lines) are different in these columns of the plots. For the theoretical predictions, solid lines use the skewness and kurtosis parameters estimated from the simulations, and dashed lines use the parameters estimated from the perturbation theory. The lines in the second columns show the first-order theory of non-Gaussianity in the analytic formula. The lines in the third columns show the second-order theory of non-Gaussianity. The rightmost columns show the differences from the first-order theory, i.e., they depict the second- and higher-order effects of non-Gaussianity in the Minkowski functionals.

As expected, the analytic predictions reproduce the results of numerical simulations when the smoothing radius

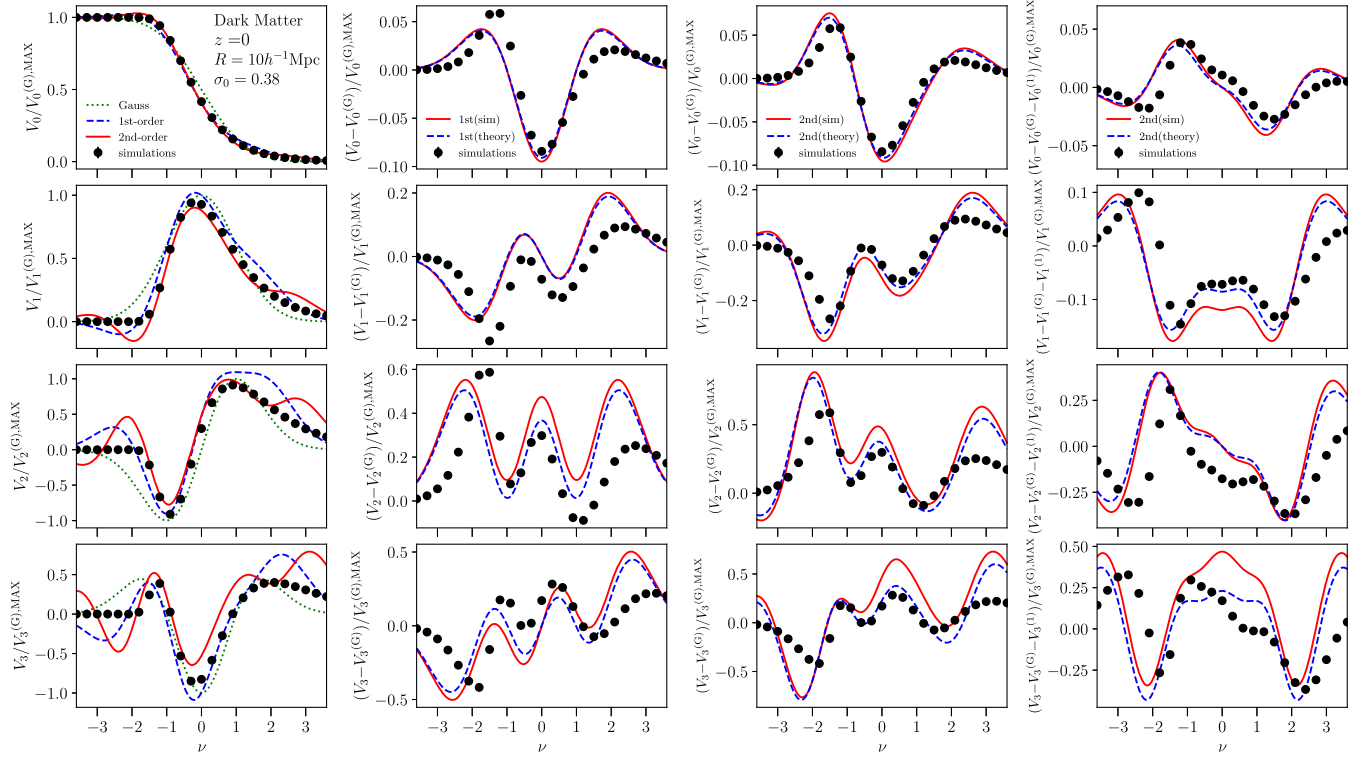


FIG. 4. Minkowski functionals calculated from the numerical simulations (points with error bars) are compared with analytic formulas. A smoothing radius $R = 10 h^{-1} \text{Mpc}$ is adopted. The panels in the leftmost column show the values of Minkowski functionals. The curves are normalized by the maximum of the absolute values for Gaussian predictions, $V_k^{(G),\text{MAX}}$. The dotted lines correspond to the zeroth-order predictions, or Gaussian predictions, dashed lines correspond to the first-order predictions, and solid lines correspond to the second-order predictions. The parameter values for the first- and second-order predictions are numerically calculated from the simulations. The panels of the second and third columns show non-Gaussian components of Minkowski functionals, i.e., Gaussian predictions are subtracted from the first columns. The numerical results (symbols) are the same in these two columns. The parameter values for the solid lines are taken from the numerical simulations, and those for the dashed lines are taken from the predictions of the perturbation theory. In the panels of the second column, the analytic predictions with the first-order theory are presented. In the panels of the third column, the analytic predictions with the second-order theory are presented. In the panels of the rightmost column, first-order predictions are subtracted from the Minkowski functionals, in order to focus on second- and higher-order effects.

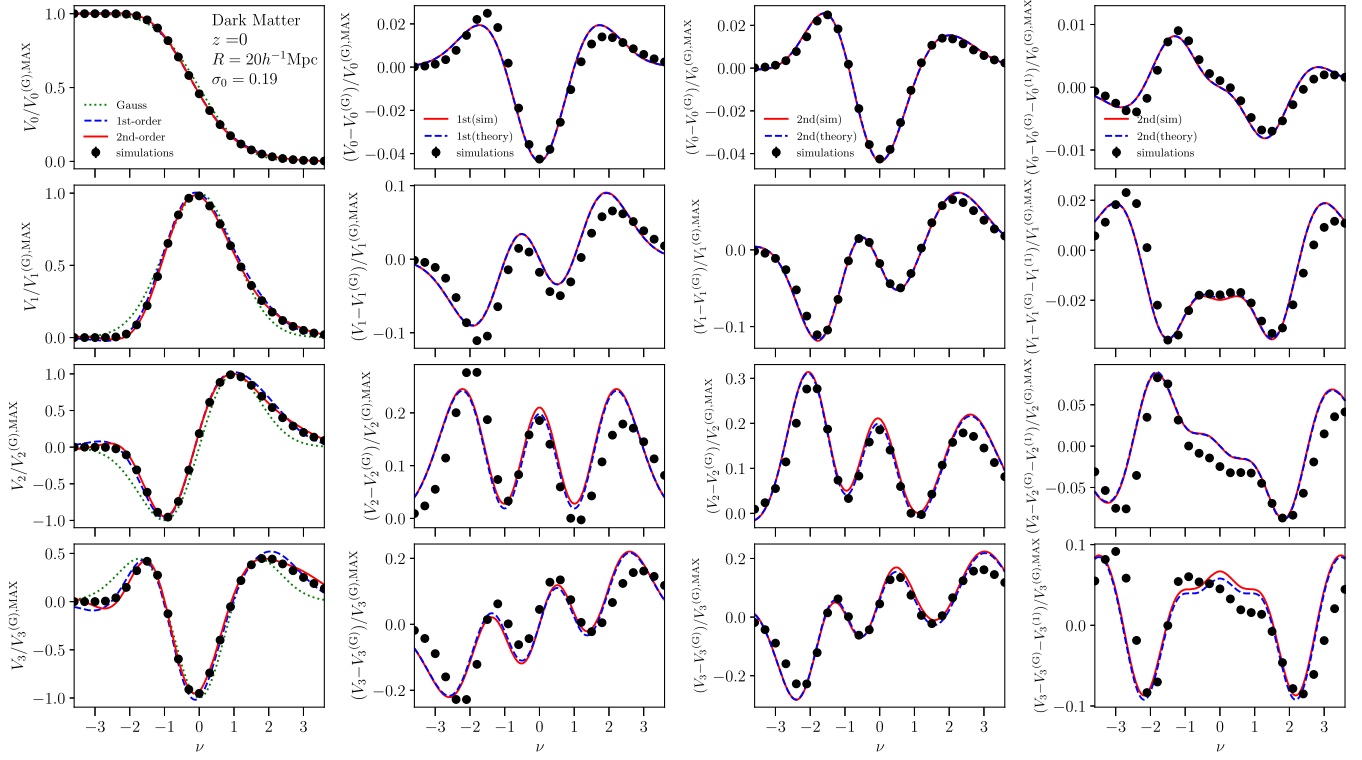


FIG. 5. Same as Fig. 4 but for the smoothing radius of $R = 20 h^{-1} \text{Mpc}$.

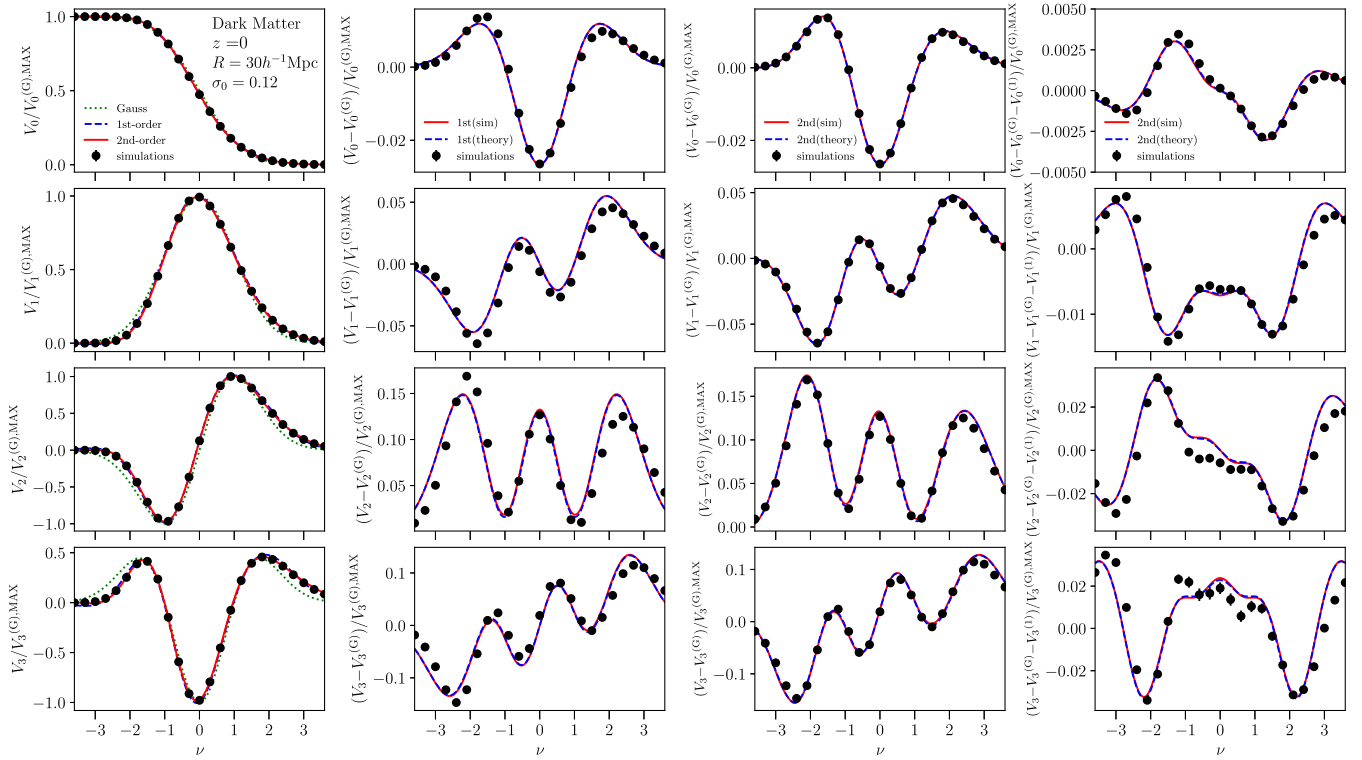


FIG. 6. Same as Fig. 4 but for the smoothing radius of $R = 30 h^{-1} \text{Mpc}$.

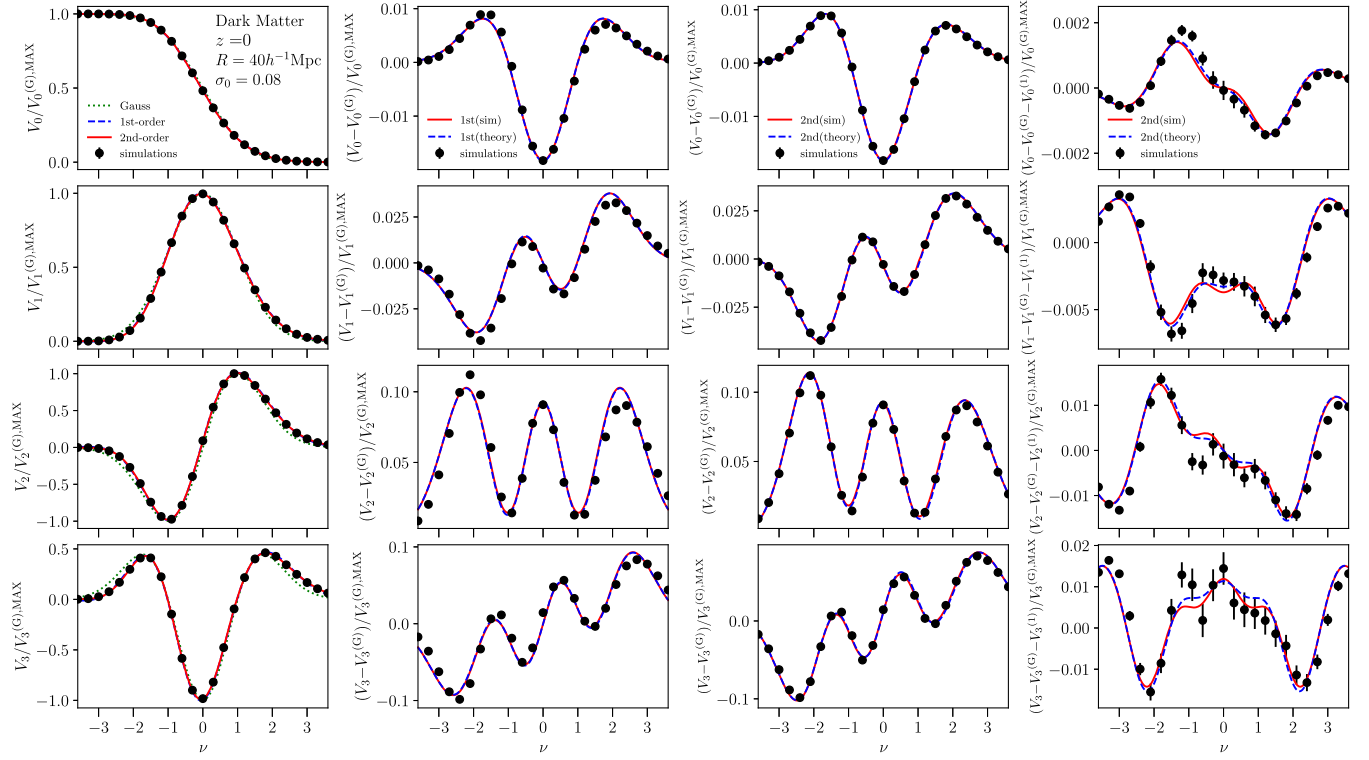


FIG. 7. Same as Fig. 4 but for the smoothing radius of $R = 40 h^{-1}$ Mpc.

is large and the expansion parameter σ_0 is small. The qualitative behaviors of the Minkowski functionals as functions of the threshold are reproduced by the analytic formulas. Quantitatively, however, the agreements are better for large smoothing radii than for small smoothing radii.

In Fig. 4 with the smallest smoothing radius of $R = 10 h^{-1}$ Mpc and $\sigma_0 = 0.38$, the theoretical predictions significantly deviate from the numerical results. The Minkowski functionals of the lower threshold, $\nu \lesssim -2$, in the numerical measurements are flat because of the negligible or zero probability of having sufficiently small or negative density $\rho/\bar{\rho} - 1 = \nu\sigma_0$ in the field. However, such constraints originate from nonperturbative effect where $|\delta_s| \gtrsim 1$ are not taken into account in the theoretical predictions with the perturbation theories. The Minkowski functionals of the higher threshold, $\nu \gtrsim 2$, are also non-perturbative and perturbation theories are not expected to apply. In the middle range of the threshold, $-2 \lesssim \nu \lesssim +2$, the second-order theory outperforms the first-order theory (compare second and third columns). There are still a certain amount of deviations between second-order theory and numerical results (fourth column) with this smoothing radius of $R = 10 h^{-1}$ Mpc. The discrepancies in the fourth column between theoretical predictions and numerical results are due to higher-order effects in the expression of the analytic formula, Eq. (9), of Minkowski functionals, and also higher-order corrections to the skewness and

kurtosis parameters estimated by the tree-level perturbation theory in the case of dashed lines.

In Fig. 5 with the smoothing radius of $R = 20 h^{-1}$ Mpc and $\sigma_0 = 0.19$, the theoretical predictions are far better than the previous case of $R = 10 h^{-1}$ Mpc. The plotted range of $-3.5 \leq \nu \leq +3.5$ satisfies $|\delta_s| \gtrsim 1$, and the perturbation theory becomes better than the previous case. The second-order theory is much better than the first-order theory as in the previous case, and deviations of the first- and second-order theories are smaller than the previous case. Therefore, the higher-order effects are relatively not so important in this case. In Figs. 6 and 7 with the smoothing radii of $R = 30 h^{-1}$ Mpc and $40 h^{-1}$ Mpc ($\sigma_0 = 0.12$ and 0.08 , respectively), the agreements of theoretical predictions and numerical results becomes better as smoothing radius increases.

Our results are consistent with the previous work [28], where one of the Minkowski functionals, the Euler characteristic among others, in the second-order theory is compared with numerical simulations of power-law primordial spectra, using measured values of kurtosis parameters, and good agreements are found for $\sigma_0 \lesssim 0.2$. Our results extend the previous work to calculating all the Minkowski functionals with arbitrary spectrum with analytic predictions of kurtosis parameters in the perturbation theory. Therefore, a condition $\sigma_0 \lesssim 0.2$ is considered as a rough criterion that the second-order theory is applicable to a certain extent, irrespective to the primordial spectrum.

V. CONCLUSIONS

In this paper, we compare the second-order formula of weakly non-Gaussian Minkowski functionals to the results of N -body simulations of the large-scale structure. As expected, the nonlinear perturbation theory reproduces the deviations from the Gaussian predictions of Minkowski functionals when the smoothing radius is large enough. We quantitatively investigate the performance of the nonlinear perturbation theory against the numerical simulations.

The nonlinear perturbation theory predicts all the parameters in the analytic formula of weakly non-Gaussian Minkowski functionals. While the calculations of skewness and kurtosis parameters with the perturbation theory involve multidimensional integrals, parts of the integrations are analytically performed, and one can numerically evaluate all the necessary integrals without any difficulty. The predicted parameters are compared with those directly evaluated by the N -body simulations in Table I and Figs. 1–3.

In our calculations, the nonlinear perturbation theory with tree-level approximations are adopted. Higher-order corrections of the perturbation theory with loop corrections may improve the theoretical predictions, while the numerical evaluations of the multidimensional integrals would be much harder. Investigations along this line is one of the possible extensions of the present work.

The Figs. 4–7 show our comparisons of the Minkowski functionals between numerical results and analytic formula for various smoothing radius. As expected, the degree of agreement varies with smoothing radius. The analytic formula is better in the larger smoothing radius (i.e., smaller σ_0), as expected. While higher-order effects of both non-Gaussianity and the perturbation theory are

simultaneously important for smaller smoothing radius, the analytic formula with larger smoothing radius outperforms the case of smaller smoothing radius.

In this paper, we only consider the clustering of dark matter in real space, and obviously ignore the effects of galaxy biasing and redshift-space distortions, which are inevitable in the actual observations of the large-scale structure of the Universe. While the purpose of this paper is to investigate the dynamically nonlinear effects on the Minkowski functionals of density fluctuations of dark matter, taking into account the biasing and redshift-space distortions should be necessary to realistically predict the shape of Minkowski functionals of observable galaxies. We will address these effects in future work. Taking into account only the biasing is not so difficult if the perturbative bias model [39] is assumed to predict the skewness and kurtosis parameters by the perturbation theory. While taking into account the redshift-space distortions in the analytic formula is tedious, much of the ground work has been done with the first-order theory of non-Gaussianity [40].

Another important application of the present work (with extensions of including the observational effects mentioned above) is to see whether or not one can distinguish the primordial non-Gaussianity from the non-Gaussianity induced by nonlinear evolutions. The method developed in this paper should offer an analytic way of investigating this kind of issue in future work.

ACKNOWLEDGMENTS

This work was supported by JSPS KAKENHI Grants No. JP19K03835 (T.M.), No. JP16K17684 (C.H.), No. JP16H02792 (S.K.), No. 21H03403 (S.K. and T.M.).

-
- [1] A. H. Guth, *Phys. Rev. D* **23**, 347 (1981).
 - [2] K. Sato, *Phys. Lett.* **99B**, 66 (1981).
 - [3] A. D. Linde, *Phys. Lett. B* **108**, 389 (1982).
 - [4] A. Albrecht and P. J. Steinhardt, *Phys. Rev. Lett.* **48**, 1220 (1982).
 - [5] J. Martin, C. Ringeval, and V. Vennin, *Phys. Dark Universe* **5**, 75 (2014).
 - [6] P. J. E. Peebles, *The Large-scale Structure of the Universe* (Princeton University Press, Princeton, NJ, 1980).
 - [7] Y. Akrami, F. Arroja *et al.* (Planck Collaboration), *Astron. Astrophys.* **641**, A9 (2020).
 - [8] H. Minkowski, *Math. Ann.* **57**, 447 (1903).
 - [9] R. Schneider, *Convex Bodies: The Brunn-Minkowski Theory* (Cambridge University Press, Cambridge, 1993).
 - [10] K. R. Mecke, T. Buchert, and H. Wagner, *Astron. Astrophys.* **288**, 697 (1994).
 - [11] J. Schmalzing and T. Buchert, *Astrophys. J. Lett.* **482**, L1 (1997).
 - [12] M. Kerscher, J. Schmalzing, J. Retzlaff, S. Borgani, T. Buchert, S. Gottlöber, V. Miller, M. Plionis, and H. Wagner, *Mon. Not. R. Astron. Soc.* **284**, 73 (1997).
 - [13] M. Kerscher, J. Schmalzing, T. Buchert, and H. Wagner, *Astron. Astrophys.* **333**, 1 (1998).
 - [14] V. Sahni, B. S. Sathyaprakash, and S. F. Shandarin, *Astrophys. J. Lett.* **495**, L5 (1998).
 - [15] J. Schmalzing, T. Buchert, A. L. Melott, V. Sahni, B. S. Sathyaprakash, and S. F. Shandarin, *Astrophys. J.* **526**, 568 (1999).
 - [16] M. Kerscher, K. Mecke, J. Schmalzing, C. Beisbart, T. Buchert, and H. Wagner, *Astron. Astrophys.* **373**, 1 (2001).
 - [17] J. V. Sheth, V. Sahni, S. F. Shandarin, and B. S. Sathyaprakash, *Mon. Not. R. Astron. Soc.* **343**, 22 (2003).

- [18] C. Hikage, J. Schmalzing, T. Buchert, Y. Suto, I. Kayo, A. Taruya, M. S. Vogeley, F. Hoyle, J. R. Gott, and J. Brinkmann, *Publ. Astron. Soc. Jpn.* **55**, 911 (2003).
- [19] S. F. Shandarin, J. V. Sheth, and V. Sahni, *Mon. Not. R. Astron. Soc.* **353**, 162 (2004).
- [20] C. Hikage, E. Komatsu, and T. Matsubara, *Astrophys. J.* **653**, 11 (2006).
- [21] M. Einasto, L. J. Liivamgi, E. Tempel, E. Saar, E. Tago, P. Einasto, I. Enkvist, J. Einasto, V. J. Martinez, P. Heinämäki, and P. Nurmi, *Astrophys. J.* **736**, 51 (2011).
- [22] Y. Liu, Y. Yu, H.-R. Yu, and P. Zhang, *Phys. Rev. D* **101**, 063515 (2020).
- [23] H. Tomita, *Prog. Theor. Phys.* **76**, 952 (1986).
- [24] T. Matsubara, *Astrophys. J. Lett.* **434**, L43 (1994).
- [25] T. Matsubara, *Astrophys. J. Suppl. Ser.* **584**, 1 (2003).
- [26] T. Matsubara, *Phys. Rev. D* **81**, 083505 (2010).
- [27] D. Pogosyan, C. Gay, and C. Pichon, *Phys. Rev. D* **80**, 081301(R) (2009); **81**, 129901(E) (2010).
- [28] C. Gay, C. Pichon, and D. Pogosyan, *Phys. Rev. D* **85**, 023011 (2012).
- [29] S. Kuriki and T. Matsubara, [arXiv:2011.04953](https://arxiv.org/abs/2011.04953).
- [30] T. Matsubara and S. Kuriki, *Phys. Rev. D* **104**, 103522 (2021).
- [31] F. Bernardeau, S. Colombi, E. Gaztaaga, and R. Scoccimarro, *Phys. Rep.* **367**, 1 (2002).
- [32] M. H. Goroff, B. Grinstein, S.-J. Rey *et al.*, *Astrophys. J.* **311**, 6 (1986).
- [33] E. L. Lokas, R. Juszkiewicz, D. H. Weinberg, and F. R. Bouchet, *Mon. Not. R. Astron. Soc.* **274**, 730 (1995).
- [34] F. Villaescusa-Navarro, C. Hahn, E. Massara *et al.*, *Astrophys. J. Suppl. Ser.* **250**, 2 (2020).
- [35] H. Hadwiger, *Vorlesungen über Inhalt, Oberfläche und Isoperimetrie* (Springer, New York, 1957).
- [36] M. W. Crofton, *Phil. Trans. R. Soc. Lond. A* **158**, 181 (1868).
- [37] J. Lesgourgues, [arXiv:1104.2932](https://arxiv.org/abs/1104.2932).
- [38] D. Blas, J. Lesgourgues, and T. Tram, *J. Cosmol. Astropart. Phys.* **07** (2011) 034.
- [39] V. Desjacques, D. Jeong, and F. Schmidt, *Phys. Rep.* **733**, 1 (2018).
- [40] S. Codis, C. Pichon, D. Pogosyan, F. Bernardeau, and T. Matsubara, *Mon. Not. R. Astron. Soc.* **435**, 531 (2013).